Electronic Supplementary Material (ESI) for Nanoscale.

Supplementary Information

Decrease in Thermal Conductivity in Polymeric P3HT Nanowires by Size-Reduction induced by Crystal Orientation: New Approaches towards Thermal Transport Engineering of Organic Materials.

Miguel Muñoz Rojo[1], Jaime Martín[1], Stéphane Grauby[2], Theodorian Borca-Tasciuc[3], Stefan Dilhaire[2] and Marisol Martín Gonzalez[1].

[1] **Instituto de Microelectrónica de Madrid,** Calle de Isaac Newton, 8 28760 Tres Cantos, Madrid, Spain.
[2] **Univ. Bordeaux, LOMA**, UMR 5798, 33405 Talence, France.
[3]**Rensselaer Polytechnique Institute**, 110 8th St, Troy, NY 12180, United States.

1. Sample Images

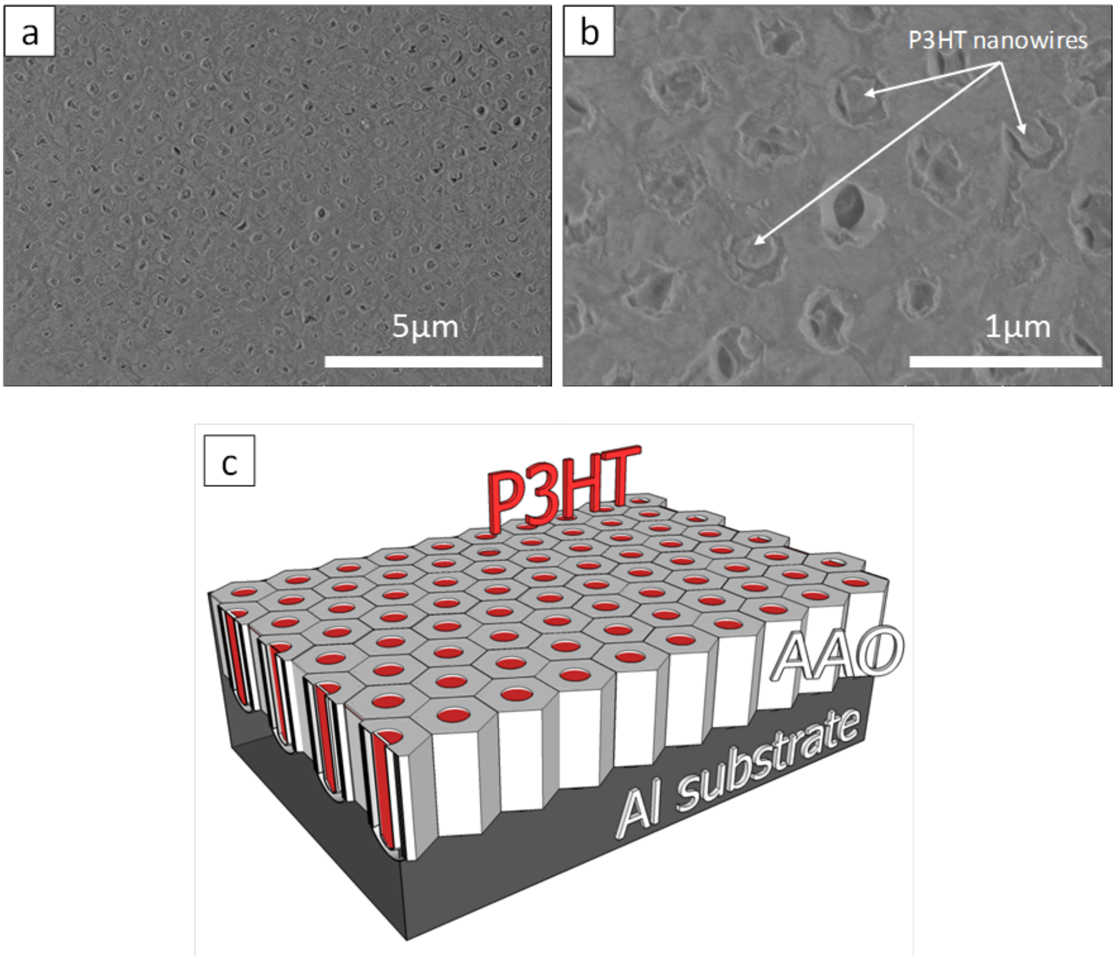

Figure S1. (a and b) SEM micrographs of surface of templates having 120 nm in diameter pores. The nanopores have been infiltrated with P3HT and the excess of P3HT film located at the AAO surfaces have been removed with a razor blade and polished with diamond paste (3 µm, Buehler MetaDi II). (c) Schematic illustration of the samples.

2. 3ω-SThM measurements.

Thermal measurements have been carried out with a 3ω-SThM working in contact mode. The probe used for this purpose is a V-shaped Pd/SiO_2, a thermoresistive probe that is sensitive to local temperatures changes with a spatial resolution limit of 60 nm [1].

In the 3ω-SThM technique, an alternating current (AC), $I(t)=I_0 \cdot sin(\omega t)$, is generated by a function generator and passed across the probe. This AC current at pulsation ω heats up the SThM tip due to Joule effect. Hence, a heat flux, P_{Joule}, at frequency 2ω is dissipated in the probe, generating a temperature variation $T_{2\omega}$ at the same pulsation. Given that the tip is in contact mode, the heat dissipates from the tip to the surface of the sample. The flow of heat dissipated depends on the thermal conductivities of the different composites of the sample scanned, which causes a tip temperature variation $T_{2\omega}$. These variations are related to the equivalent thermal resistance, R_{eq}, between the tip and the sample. The higher the temperature variations $T_{2\omega}$, the lower the sample thermal conductivity.

Since the tip is a thermoresistive probe, the tip temperature variation at 2ω induces a tip resistance variation at the same pulsation 2 ω. Then, according to Ohm's law, the tip voltage, which is measured thanks to a lock-in amplifier, varies at 3ω and is then related to the thermal conductivity of the scanned sample area[2].

The tip voltage amplitude at 3ω can be expressed mathematically as [1, 3, 4] ,

$$(V_{3\omega})_{tip} = K_{ampli}\frac{R_{tip}\alpha_{tip}I_0}{2} < T_{2\omega} > \tag{1}$$

where K_{ampli} is the amplification system gain, I_0 is the amplitude of the ω pulsation current supplying to the probe, and $< T_{2\omega} >$ is the mean temperature variation amplitude over the tip length.

The 3ω-SThM technique makes simultaneously a topographic images and 3ω-voltage image of the sample surface. This last image is usually called conductivity contrast imaging or thermal map because of the information given by the $(V_{3\omega})_{Tip}$ is co-related to $< T_{2\omega} >$ through equation (1) and so to the equivalent tip-sample thermal resistance R_{eq} map. In order to obtain the relation between the mean tip temperature variation, $< T_{2\omega} >$, and the equivalent thermal resistance, R_{eq}, it is necessary to determine carefully different parameters related mainly with the probe [1]. Figure S2 shows a schematic view of the experimental set-up.

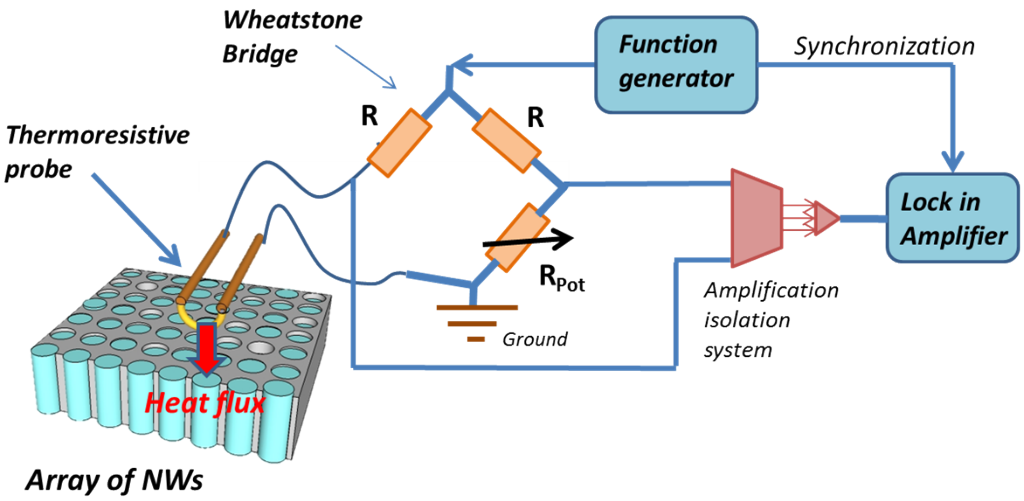

Figure S2. Schematic view of the set-up of a 3ω-SThM.

An important parameter that must be considered to analyze the thermal conductivity of NWs from the equivalent thermal resistance measured, as well as to determine the thermal lateral resolution of the probe, is the thermal exchange radius of the tip, r_{ex}. For that purpose, we follow the experimental process described in ref. [1] , where a thermal scan over an abrupt step made of thick oxide layer on Si substrate is carried out. From the analysis of the $V_{3\omega}$ signal at the edges of this step the thermal exchange radius of the tip can be determined. The tip used to measure P3HT NWs embedded in a matrix resulted into r_{ex}=175±10 nm for 350nm and 220nm diameter NWs and r_{ex}=81±5 nm for 120nm diameter NWs. This variation in the thermal exchange radius of the tip justifies the necessity to calibrate it at regular intervals since this estimation constitutes an essential value in our method in order to determine reliable value of the thermal conductivity.

3. **WAXS experimental set-up.**

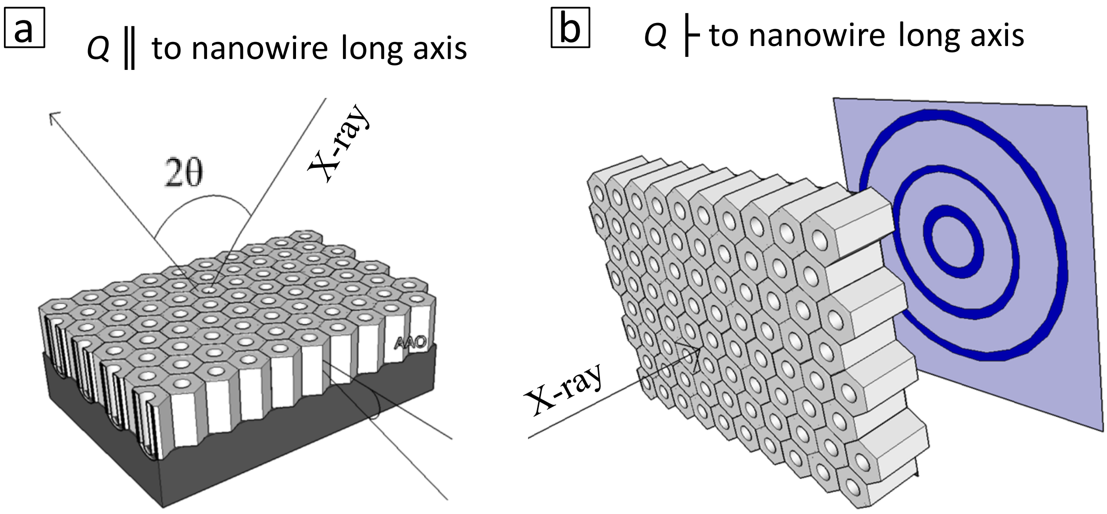

Figure S3. Schematic representations of WAXS experiments: (a) Experiment in reflection geometry in which the wave vector *Q* is parallel to pore long axis.(b) Experiment in transmission geometry. The X-ray beam travels along the direction perpendicular to the template surface, in such a way that *Q* is nearly perpendicular to the pore long axis.

4. **WAXS diffractograms of bulk P3HT.**

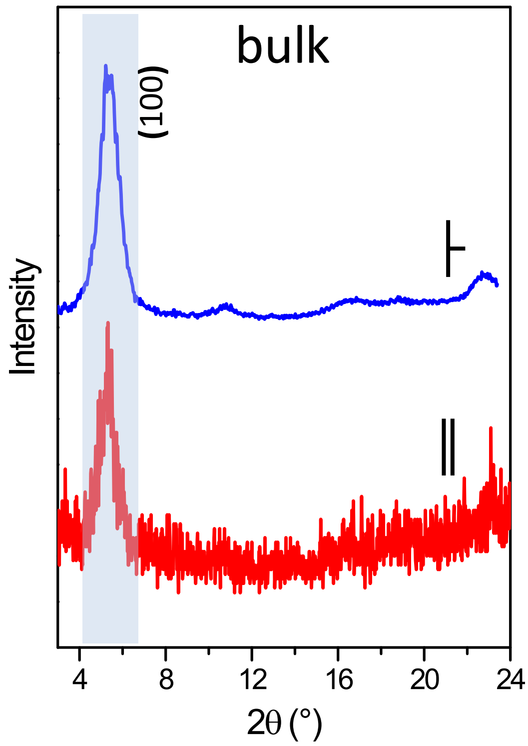

Figure S4. WAXS diffractograms of bulk (powder) P3HT nanowires in which the wave vector, *Q,* was parallel (red line) and perpendicular (blue line) to sample surface.

For the bulk sample, the P3HT was powdered in an Agatha mortar in order to ensure the isotropic orientation of crystals in this sample.

5. Validation of the effective medium theory with COMSOL Multiphysic´s simulation.

In order to prove the validity of the effective medium theory from which the thermal conductivity of the NWs have been determined, we have carried out with a COMSOL Multiphysic® simulation to analyze the experimental measurements.

Our simulation consists of three different P3HT nanowire arrays embedded in alumina with 350nm, 220nm and 120nm diameters. From the geometrical point of view, the total sample area considered is 36µm2 but in order to increase the simulation speed, we have taken advantage of the symmetry of the sample. Hence, only a fourth of the total sample has been taken into account but adding symmetry boundary conditions in its internal walls. The proper functioning of the symmetry has been checked with a comparison of their results with the ones obtained for a full sample simulation. The exterior walls are considered as open boundaries that limit the modeling domain that extends in an open fashion within the temperature variable, *T*, obtained in this limit. The sample is 5µm long and its bottom temperature has been fixed at room temperature (293.15ºK). The areal packing density has been kept identical to the ones considered in our manuscript (see Table I of the manuscript). A convection heat coefficient on the top surface of h=5 $W/K\cdot m^2$ to simulate the effects of the surrounding air is considered. Concerning the properties of the materials, the thermal conductivity of the solid part of the alumina is fixed to 1.38 W/K·m while the thermal conductivity of the nanowires will be varied.

In order to simulate the heating of the SThM probe, we have defined a circular Gaussian heat source with an applied power of $1\cdot10^{-5}$W. This distribution of heat has been considered in similitude to the measurements of the thermal exchange radius given in reference[1]. The same thermal exchange radius as the one given in Table I of the manuscript has been taken for each sample.

This heat source is placed on top of the nanowires and on the alumina matrix between the nanowires in similitude to the experimental measurements carried out with our SThM system. The maximum temperature reached at each location is considered and the thermal resistance for the nanowire, $R_{therm\,NW}^{simul}$, and the alumina, $R_{therm\,AAO}^{simul}$, are obtained by using the next equation,

$$R_{therm}^{simul} = \frac{T_{max} - T_{room}}{\dot{Q}} \quad (1)$$

This process has been performed in each nanowire diameter sample. Figure S5 shows an example of the simulation obtained for 300nm diameter nanowire array embedded in alumina matrix.

To perform this simulation, we used the "Heat Transfer in Solids" module in COMSOL Multiphysics® and solve the stationary equation of heat for solids. In order to run the simulation accurately, the mesh was refined in each nanowire array samples until no variation in the results were observed. The results are sensitive to the mesh especially as the diameter of the nanowire is reduced.

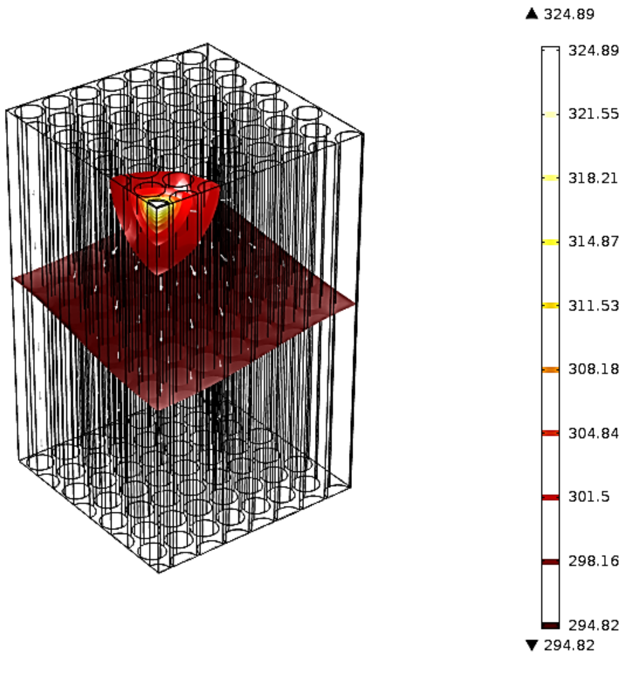

Figure S5. Temperature iso-surfaces and total heat flow (arrows) when the heat source is positioned on top of a 300nm diameter nanowire.

First of all, validation of the model was carried out for a bulk sample with different thermal conductivities and a bulk sample with nanowires, having both the same thermal conductivity, using the equation: $R_{therm\,theory} = \frac{1}{4 \cdot r_{th} \cdot k}$. Table I shows that the model works properly, within 5% error maximum, for a thermal exchange radius of 175nm and 81nm.

Table I. Validation of the model. Simulated results versus the expected ones $R_{therm} = \frac{1}{4 \cdot r_{th} \cdot k}$ for r_{th} of 175 nm and 81 nm.

k_{bulk} (W/K·m)	r_{th} (nm)	$R_{therm\,simul}$ (W/K)	$R_{therm\,theo}$ (W/K)
0,1	175	1,42E+07	1,43E+07
0,5	175	2,83E+06	2,86E+06
1	175	1,42E+06	1,43E+06
1,5	175	9,44E+05	9,52E+05
2	175	7,08E+05	7,14E+05
2,5	175	5,66E+05	5,71E+05
3	175	471873	4,76E+05
3,5	175	404462,5	4,08E+05
4	175	353904,75	3,57E+05
4,5	175	314582	3,17E+05
5	175	283123,75	2,86E+05
0,1	81	3,00E+07	3,09E+07
0,5	81	5,99E+06	6,17E+06
1	81	3,00E+06	3,09E+06
1,5	81	2,00E+06	2,06E+06
2	81	1,50E+06	1,54E+06
2,5	81	1,20E+06	1,23E+06
3	81	998463	1,03E+06
3,5	81	855824,5	8,82E+05
4	81	748847,75	7,72E+05
4,5	81	665641,75	6,86E+05
5	81	599078,25	6,17E+05

After the validation has been achieved, it is decided to analyze the thermal resistance obtained in the alumina matrix and on top of the nanowires. On the one hand, by subtracting the simulated equivalent thermal resistance of the alumina and the alumina experimental thermal resistance given in Table I of the manuscript, the simulated contact resistance is obtained: $R_C^{simul} = R_{therm\,AAO}^{exper} - R_{therm\,AAO}^{simul}$. On the other hand, by subtracting the simulated contact resistance to the experimental nanowires resistance, $R^{experm}_{therm\,NW}$ of Table I of the manuscript, $R_{NW} = R^{exper}_{therm\,NW} - R^{simul}_{C}$, it would be possible to compare the simulated nanowire resistance with the one just calculated. By varying the thermal conductivity of the nanowire until we fit these thermal resistances, we would be able to determine the intrinsic thermal conductivity of the nanowire. The next tables and figures show the results given from the simulation and its comparison to the effective medium theory results for the three different NWs arrays samples, where $R^{exp.}_{C} = R^{experm}_{AAO\,therm} - R^{Simulated}_{AAO\,therm}$, $R^{mean\,eff.}_{C} = R^{experm}_{AAO\,therm} - 1/(4 \cdot k_{AAO} \cdot r_{th})$, $R^{exp.+sim}_{NW\,therm} = R^{experm}_{NW\,therm} - R^{exp.}_{C}$ and $R^{mean\,eff.+sim}_{NW\,therm} = R^{experm}_{NW\,therm} - R^{mean\,eff.}_{C}$.

Table II. Data results for the 350nm diameter NW array sample. Thermal exchange radius used is 175nm.

k_{NW} (W/K·m)	$R^{Simula}_{NW\,the}$ (W/K)	$R^{effec}_{NW\,th}$ (W/K)	$R^{Simul}_{AAO\,t}$ (W/K)	$R^{expe}_{NW\,t}$ (W/K)	R^{expe}_{AAO} (W/K)	$R^{exp.}_{C}$ (W/K)	R^{mean}_{C} (W/K)	$R^{ex+ps.im}_{NW\,th}$ (W/K)	$R^{mean+sei}_{NW\,th}$ (W/K)
0,1	2,50E+06	2,11E+06	1,24E+06	4,36E+06	4,63E+06	3,39E+06	3,59E+06	965360,25	765196,687
0,5	1,67E+06	1,59E+06	1,11E+06	4,36E+06	4,63E+06	3,52E+06	3,59E+06	840183,75	765196,687
1	1,22E+06	1,22E+06	1,05E+06	4,36E+06	4,63E+06	3,58E+06	3,59E+06	778212,25	765196,687
2	835250	830082,178	996767,75	4,36E+06	4,63E+06	3,63E+06	3,59E+06	726767,75	765196,687
3	655500	629049,506	973690,75	4,36E+06	4,63E+06	3,66E+06	3,59E+06	703690,75	765196,687
4	549750	506406,036	960459,25	4,36E+06	4,63E+06	3,67E+06	3,59E+06	690459,25	765196,687
5	479250	423782,684	951838	4,36E+06	4,63E+06	3,68E+06	3,59E+06	681838	765196,687

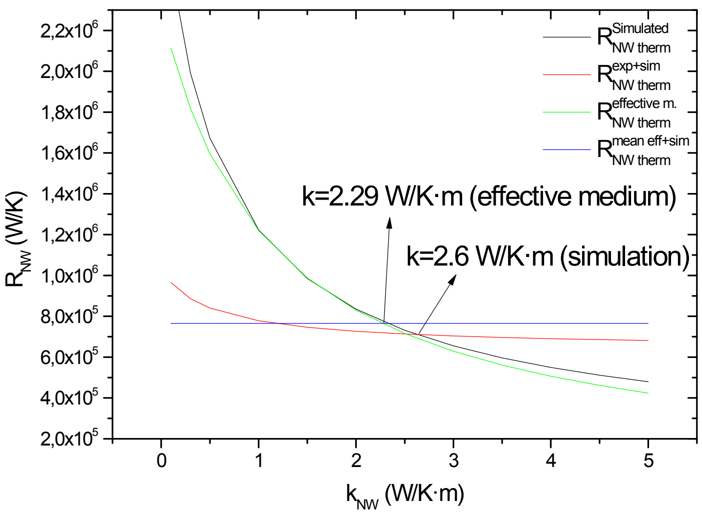

Figure S6. Simulation and effective medium results for 350nm diameter NWs sample.

Table III. Data results for the 220nm diameter NW array sample. Thermal exchange radius used is 175nm.

k_{NW} (W/K·m)	$R^{Simula}_{NW\ the}$ (W/K)	$R^{effec}_{NW\ th}$ (W/K)	$R^{Simul}_{AAO\ t}$ (W/K)	$R^{expe}_{NW\ t}$ (W/K)	R^{expe}_{AAO} (W/K)	$R^{exp.}_{C}$ (W/K)	R^{mean}_{C} (W/K)	$R^{exp+sim}_{NW\ th}$ (W/K)	$R^{mean+sei}_{NW\ th}$ (W/K)
0,1	1,32E+06	1,35E+06	1,09E+06	4,49E+06	4,34E+06	3,25E+06	3,30E+06	1,24E+06	1,19E+06
0,5	1,20E+06	1,23E+06	1,05E+06	4,49E+06	4,34E+06	3,29E+06	3,30E+06	1,20E+06	1,19E+06
1	1,10E+06	1,11E+06	1,03E+06	4,49E+06	4,34E+06	3,31E+06	3,30E+06	1,18E+06	1,19E+06
2	960500	930665,426	996967	4,49E+06	4,34E+06	3,34E+06	3,30E+06	1,15E+06	1,19E+06
3	869500	800320,128	980512,25	4,49E+06	4,34E+06	3,36E+06	3,30E+06	1,13E+06	1,19E+06
4	801750	702000,702	969519,75	4,49E+06	4,34E+06	3,37E+06	3,30E+06	1,12E+06	1,19E+06
5	748750	625195,374	961505,5	4,49E+06	4,34E+06	3,38E+06	3,30E+06	1,11E+06	1,19E+06

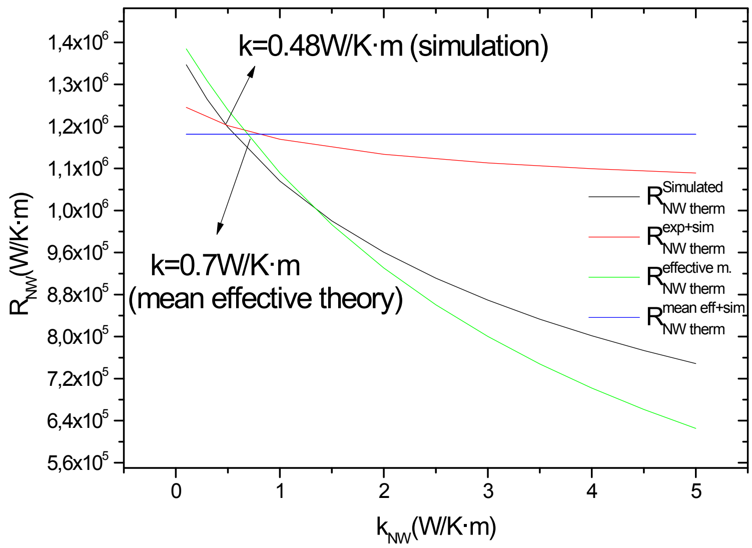

Figure S7. Simulation and effective medium results for 220nm diameter NWs sample.

Table IV. Data results for the 120nm diameter NW array sample. Thermal exchange radius used is 81nm.

k_{NW} (W/K·m)	$R^{Simula}_{NW\ the}$ (W/K)	$R^{effec}_{NW\ th}$ (W/K)	$R^{Simul}_{AAO\ t}$ (W/K)	$R^{expe}_{NW\ t}$ (W/K)	R^{expe}_{AAO} (W/K)	$R^{exp.}_{C}$ (W/K)	R^{mean}_{C} (W/K)	$R^{exp+sim}_{NW\ th}$ (W/K)	$R^{mean+sei}_{NW\ th}$ (W/K)
0,1	2,58E+06	2,42E+06	2,436E+06	6,48E+06	6,36E+06	3,924E+06	4,12E+06	2,556E+06	2,36E+06
0,5	2,42E+06	2,36E+06	2,428E+06	6,48E+06	6,36E+06	3,931E+06	4,12E+06	2,548E+06	2,36E+06
1	2,27E+06	2,29E+06	2,423E+06	6,48E+06	6,36E+06	3,937E+06	4,12E+06	2,543E+06	2,36E+06
2	2,04E+06	2,16E+06	2,415E+06	6,48E+06	6,36E+06	3,945E+06	4,12E+06	2,535E+06	2,36E+06
3	1,87E+06	2,04E+06	2,409E+06	6,48E+06	6,36E+06	3,95E+06	4,12E+06	2,529E+06	2,36E+06
4	1,75E+06	1,94E+06	2,406E+06	6,48E+06	6,36E+06	3,954E+06	4,12E+06	2,526E+06	2,36E+06
5	1,65E+06	1,85E+06	2,403E+06	6,48E+06	6,36E+06	3,957E+06	4,12E+06	2,523E+06	2,36E+06

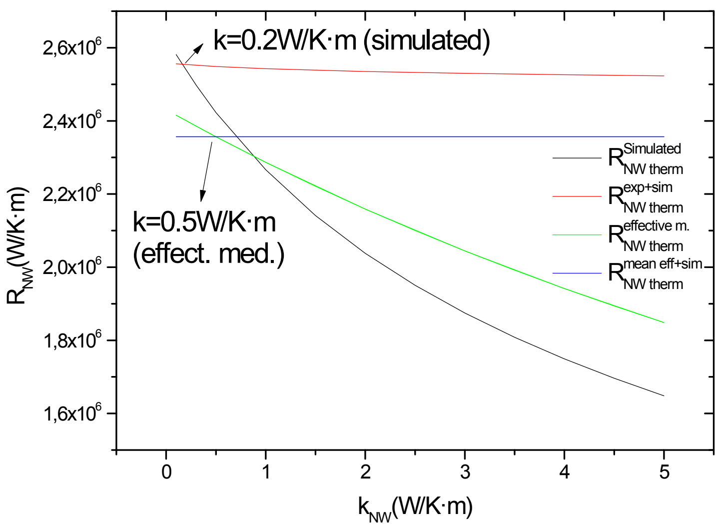

Figure S8. Simulation and effective medium results for 120nm diameter NWs sample.

.

If we compare the results obtained from the simulation to the ones expected by the effective medium theory, we can conclude that the effective medium theory is working reasonably in our case. Table V summarizes these results.

Table V. Comparison between thermal conductivity values obtained with the effective medium theory and the COMSOL Multiphysic® simulation.

NW diameter (nm)	k_{NW} (Effective medium theory) W/(K·m)	k_{NW} (Simulation) W/(K·m)
350	2.29±0.15	2.6
220	0.70±0.12	0.48
120	0.50±0.24	0.2

References

1. Puyoo, E.; Grauby, S.; Rampnoux, J.-M.; Rouviere, E.; Dilhaire, S. *Review of Scientific Instruments* **2010,** 81, (7), 073701-5.
2. Cahill, D. *Review of scientific instruments* **1990,** 61, (2), 802-808.
3. Puyoo, E.; Grauby, S.; Rampnoux, J.-M.; Rouviere, E.; Dilhaire, S. *Journal of Applied Physics* **2011,** 109, (2), 024302-9.
4. Muñoz-Rojo, M.; Grauby, S.; Rampnoux, J. M.; Caballero-Calero, O.; Martin-Gonzalez, M.; Dilhaire, S. *Journal of Applied Physics* **2013,** 113, (5), 054308-7.